

Article

The Reaction of HO₂ and CH₃O₂: CH₃OOH Formed from the Singlet Electronic State Surface

 Thanh Lam Nguyen  and John F. Stanton *

Quantum Theory Project, Departments of Chemistry and Physics, University of Florida, Gainesville, FL 32611, USA

* Correspondence: johnstanton@ufl.edu

Abstract: High-level coupled-cluster calculations in combination with two-dimensional master equation simulations were used to study the HO₂ + CH₃O₂ reaction, which plays an important role in the oxidation of methane and hydrocarbons in the Earth's atmosphere and low-temperature combustion. The main reaction pathways taking place on the lowest-lying triplet and singlet potential energy surfaces (PES) were characterized. Interestingly, methyl hydroperoxide (CH₃OOH), the sole product, could be produced from both the triplet and singlet PESs, with a ratio of roughly 9:1. Formaldehyde is not made as a primary product, but can be formed via secondary chemistry. The formation of methyl tetraoxide (MTO) from the singlet PES is unimportant. The calculated reaction rate coefficients were found to be practically pressure-independent for $p \leq 760$ Torr and can be given by $k(T) = 2.75 \times 10^{-13} \times e^{+1.75 \text{ kcal mol}^{-1}/RT}$ (in cm³/s), an expression useful for kinetics modeling over the range $T = 200\text{--}800$ K. The rate constant has a slight negative Arrhenius energy dependence of about $-1.75 \text{ kcal mol}^{-1}$, falling about a factor of 30 from 200 K to 800 K.

Keywords: kinetics; SCTST; 2DME; CH₃OOH; HO₂; CH₃O₂



Citation: Nguyen, T.L.; Stanton, J.F. The Reaction of HO₂ and CH₃O₂: CH₃OOH Formed from the Singlet Electronic State Surface. *Atmosphere* **2022**, *13*, 1397. <https://doi.org/10.3390/atmos13091397>

Academic Editor: Anthony Joseph Hynes

Received: 12 August 2022

Accepted: 29 August 2022

Published: 30 August 2022

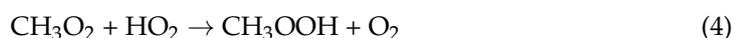
Publisher's Note: MDPI stays neutral with regard to jurisdictional claims in published maps and institutional affiliations.



Copyright: © 2022 by the authors. Licensee MDPI, Basel, Switzerland. This article is an open access article distributed under the terms and conditions of the Creative Commons Attribution (CC BY) license (<https://creativecommons.org/licenses/by/4.0/>).

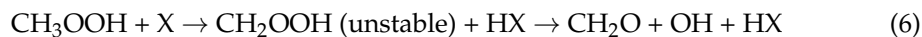
1. Introduction

Methane is the simplest stable hydrocarbon and is released in tremendous quantities into the Earth's atmosphere from both natural (biogenic) and anthropogenic processes [1–3]. In the atmosphere, it is mainly oxidized by highly reactive hydroxyl radical (OH) via Equation (1) to yield methyl radical (CH₃), followed by the association of CH₃ with oxygen molecule (O₂) to make methyl peroxy radical (CH₃O₂) via Equation (2) [4–8]. In polluted environments (i.e., urban or industrial areas) where NO_x concentrations are high, CH₃O₂ radicals primarily react with NO via Equation (3) to yield CH₃O and NO₂. Subsequent photolysis of NO₂ will then lead to the formation of tropospheric ground-level ozone, which is a contributor to smog, harmful to both animal and plant life. However, in clean environments (such as rural or forest areas), CH₃O₂ is mainly consumed by reacting with HO₂ radicals (Equations (4) and (5)) [4–8]. The same sequential reaction steps are expected to occur in the flames of CH₄ (or hydrocarbons) at low temperatures.



It is well established that the title reaction mainly (if not exclusively) produces methyl hydroperoxide (CH₃OOH) via Equation (4) [9–19]. Conversely, the formation of formaldehyde (CH₂O) via Equation (5) remains debated. Some experiments [12,19] have found

CH₂O while others [13–15] did not. It is widely believed that the production of CH₂O is at most minor, less than 10% [3,13]. It should be mentioned that the CH₂O observed in some experiments could be produced (as a secondary product) through the (photo-) oxidation processes of the primary product CH₃OOH, Equations (6) and (7).



Earlier, the title reaction was theoretically studied using CCSD(T)//B3LYP [20,21] and CASPT2//CASCF [22] levels of theory. Both the lowest-lying triplet and singlet electronic state potential energy surfaces (PES) were characterized [20,22]. The reaction pathway taking place on the triplet PES to yield CH₃OOH (Equation (4)) was reported to be dominant while the contribution of the singlet PES was postulated to be negligibly small [20,22]. The potential catalytic role of one water molecule was also investigated, but found to be insignificant [23,24]. The reaction rate coefficients were computed by assuming the thermal equilibrium condition [22], which can only be achieved at extremely high pressures. Such conditions cannot be fulfilled in the Earth's atmosphere and in experiments for this reaction system, which features a shallow well (i.e., van der Waals complex) and a submerged TS (see Figure 1). The title reaction as displayed in Figure 1 is expected to be (slightly) pressure-dependent above 1 atm. In such a case, solving a master equation is required to obtain the reaction rate constants.

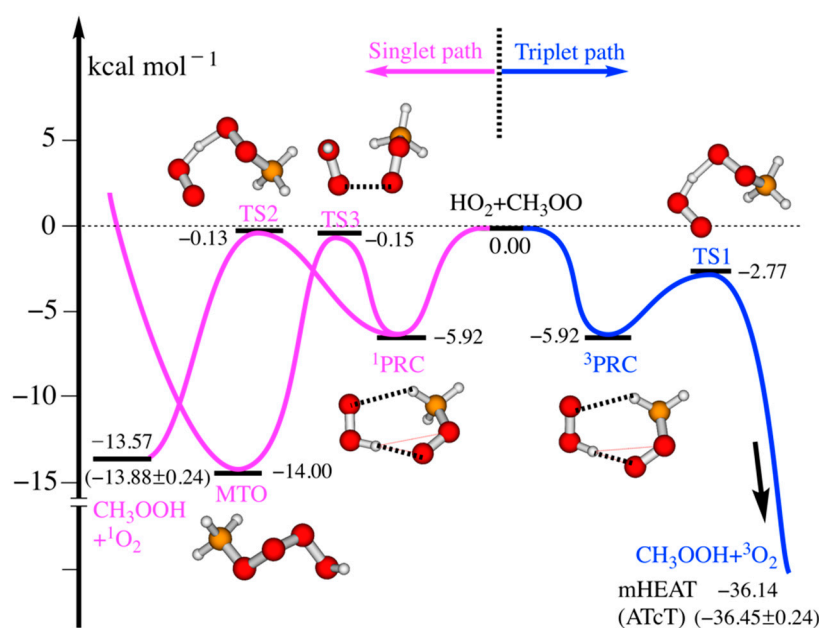


Figure 1. Schematic reaction energy profiles for the reaction of HO₂ and CH₃O₂, constructed using the mHEAT method (see text). The left-hand side shows the important reaction pathways on the singlet PES while the right-hand side displays the reaction pathway on the triplet PES. Benchmark ATcT values (in parentheses) are also included for comparison.

In this work, the title reaction is restudied using high-level accuracy coupled-cluster calculations. We reexamine the potential roles of the singlet PES; particularly, we address questions of the potential formation of methyl tetraoxide (MTO, CH₃OOOOH), methyl peroxide (CH₃OOH), and formaldehyde from the singlet PES. We then solve an E,J-resolved master equation for the temperature range 200–800 K and a pressure range of 1–1000 Torr (i.e., conditions applicable to the Earth's atmosphere and low-temperature combustion processes) to quantify product branching ratios and to provide reliable phenomenological rate constants for kinetics modeling.

2. Theoretical Methodologies

2.1. High-Level Coupled-Cluster Calculations

The radical–radical association of HO₂ and CH₃O₂ can, in principle, take place on both the lowest-lying triplet and singlet PESs. The geometries of all key stationary points were fully optimized using the frozen-core (fc) CCSD(T) method [25–27] in combination with a triple-zeta atomic natural orbital (ANO1) [28,29] basis set. As usual, unrestricted and restricted Hartree–Fock reference wave functions in the CCSD(T) calculations were used for triplet and singlet stationary points, respectively. However, for singlet open-shell structures (such as TS2, TS3, and ¹PRC, see Figure 1), broken-symmetry UHF reference wave functions were used. Harmonic vibrational frequency analyses were then carried out to verify the located stationary points as well as to compute harmonic force fields. To obtain anharmonic zero-point vibrational energy (ZPE) corrections and anharmonic constants for subsequent kinetics simulations, cubic and quartic force constants were also computed using fc-CCSD(T)/aug-cc-pVDZ [30] level of theory.

Total electronic energies (including anharmonic ZPE corrections) of all stationary points were then obtained with the composite mHEAT-345(Q) method. As detailed elsewhere, the mHEAT-345(Q) protocol [31] generally comprises a series of high-level (single-point energy) coupled-cluster calculations; it recovers a large part of electron correlation with the perturbative triple excitations method (CCSD(T)) and a smaller part of electron correlation with the fully iterative triple (CCSDT) and non-iterative (perturbative) quadruple (CCSDT(Q)) methods [31]. In addition, other smaller corrections include the diagonal Born–Oppenheimer correction (DBOC), scalar relativity, and spin-orbit [31]. As seen in Figure 1, mHEAT calculations provide a high accuracy (relative) energy of about ±0.3 kcal mol^{−1} as compared to benchmark ATcT [32] for the reaction enthalpies. Although experimental activation energies are not available to be compared with the theory in this circumstance, a (conservative) accuracy energy of ± 1.0 kcal mol^{−1} may be expected for other stationary points.

The calculations made for the a¹Δ_g state of ¹O₂ (an RHF-based treatment starting from the b¹Σ_g⁺ state) are clearly not adequate (as evidenced by the fairly large discrepancy with ATcT), but it should be emphasized that the thermodynamic energy of this species is not important for the kinetics calculations presented in this work. Nevertheless, the (relative) energy of the a¹Δ_g state of ¹O₂ is estimated using the energy of triplet ground state of O₂ obtained with the mHEAT method and a singlet-triplet energy gap of 22.57 ± 0.24 kcal mol^{−1} taken from ATcT [32].

A comparison of relative energies of various stationary points calculated with the mHEAT method in this work and values obtained with lower levels of theory reported in the literature are given in Table 1. A difference of a few kcal mol^{−1} can be seen there. To the best of our knowledge, the mHEAT method used in this work is the highest level of theory that has ever been applied to the title reaction. It is well known that kinetic results are sensitively dependent on the accuracy of the calculated barrier heights. Therefore, high-accuracy relative energies are required for the following kinetic analysis.

Table 1. A comparison of relative energies (in kcal mol⁻¹) of various stationary points for the title reaction occurring on the triplet and singlet PESs calculated with mHEAT method and values in the literature.

Species	mHEAT	Anglada et al. ^(b)	Zhang et al. ^(c)	Hou et al. ^(d)
³ PRC	-5.92 ± 0.5	-4.5	-5.99	-7.65
³ TS1	-2.77 ± 0.5	-3.8	-2.24	-3.76
¹ PRC	-5.92 ± 1.0	-4.9	n/a	n/a
¹ TS2	-0.13 ± 1.0	5.5	10.72	8.24
¹ TS3	-0.15 ± 1.0	-1.8	n/a	n/a
¹ CH ₃ OOOOH	-14.00 ± 0.5	-6.4	-11.29	-9.22
CH ₃ OOH + ³ O ₂	-36.14 ± 0.5 ^(a)	-36.9	-36.08	-37.82
CH ₃ OOH + ¹ O ₂	-13.57 ± 0.5 ^(a)	-12.6	-5.37	-6.93

^(a) Benchmark ATcT values [32] are -36.45 ± 0.24 kcal mol⁻¹ for CH₃OOH + ³O₂ and -13.88 ± 0.24 kcal mol⁻¹ for CH₃OOH + ¹O₂. ^(b) Calculated at CASPT2/6-311+G(3df,2p)//CASSCF level of theory [22]. ^(c) Obtained with CCSD(T)/6-311+G(3d,2p)//B3LYP level of theory [23]. ^(d) Reported using CCSD(T)/cc-pVDZ//B3LYP level of theory [20].

2.2. Two-Dimensional Master Equation Calculations

As shown in Figure 1, the title reaction proceeds via energized adducts (pre-reactive complex (PRC) and methyl tetraoxide (MTO)) before leading to products; it is therefore expected to depend on pressure. As a result, a master equation approach must be used to compute phenomenological rate constants as functions of temperature and pressure. An E,J-resolved master equation [33–39] for a chemically activated reaction (see Figure 1), which describes the competition of unimolecular dissociation reactions and energy transfer processes through collisions between a bath gas and vibrationally excited intermediates as a function of time, can be expressed by Equation (8) for the reaction pathway on the triplet PES and in Equation (9) for the reaction pathways on the singlet PES.

On the triplet PES

$$\frac{\partial C_3(E_m, J_m)}{\partial t} = \int_{E_n=0}^{E_{max}} \sum_{J_n=0}^{J_{max}} P_n((E_m, J_m | E_n, J_n) \cdot \omega_{LJ} \cdot C_3(E_n, J_n) \cdot dE_n - \omega_{LJ} \cdot C_3(E_m, J_m) - \{k_{3 \rightarrow CH_3O_2}(E_m, J_m) + k_{3 \rightarrow CH_3OOH}(E_m, J_m)\} \cdot C_3(E_m, J_m) + OST_3(E_m, J_m)) \quad (8)$$

On the singlet PES

$$\begin{aligned} \frac{\partial C_1(E_m, J_m)}{\partial t} &= \int_{E_n=0}^{E_{max}} \sum_{J_n=0}^{J_{max}} P_n((E_m, J_m | E_n, J_n) \cdot \omega_{LJ} \cdot C_1(E_n, J_n) \cdot dE_n - \omega_{LJ} \cdot C_1(E_m, J_m) \\ &\quad - \{k_{1 \rightarrow CH_3O_2}(E_m, J_m) + k_{1 \rightarrow CH_3OOH}(E_m, J_m) + k_{1 \rightarrow 2}(E_m, J_m)\} \\ &\quad \cdot C_1(E_m, J_m) + k_{2 \rightarrow 1}(E_m, J_m) \cdot C_2(E_m, J_m) + OST_1(E_m, J_m)) \\ \frac{\partial C_2(E_m, J_m)}{\partial t} &= \int_{E_n=0}^{E_{max}} \sum_{J_n=0}^{J_{max}} P_n((E_m, J_m | E_n, J_n) \cdot \omega_{LJ} \cdot C_2(E_n, J_n) \cdot dE_n - \omega_{LJ} \cdot C_2(E_m, J_m) \\ &\quad - k_{2 \rightarrow 1}(E_m, J_m) \cdot C_2(E_m, J_m) + k_{1 \rightarrow 2}(E_m, J_m) \cdot C_1(E_m, J_m)) \end{aligned} \quad (9)$$

Here 1, 2, and 3 designate for singlet PRC, MTO, and triplet PRC, respectively. In Equations (8) and (9), J_{max} is the maximum angular momentum; E_{max} is the maximum internal energy; $C_3(E_m, J_m, t)$ represents the (time-dependent) mole fractions of triplet PRC in the state (E_m, J_m) and time t ; ω_{LJ} (in s⁻¹) is the Lennard–Jones collisional frequency [40–42]; and $k_{1 \rightarrow 2}(E_m, J_m)$ (in s⁻¹) is the (E_m, J_m) -resolved microcanonical rate coefficient for the isomerization step of singlet PRC to MTO. $P_3(E_m, J_m | E_n, J_n)$ is the E,J-resolved collisional transfer probability distribution function of triplet PRC from the state (E_n, J_n) to state (E_m, J_m) . OST stands for the original source term, and is given by [43–46]:

$$OST_3(E_m, J_m) = F_3(E_m, J_m) \cdot k_{3,\infty}(T) \cdot [HO_2] \cdot [CH_3O_2], \quad (10)$$

$$OST_1(E_m, J_m) = F_1(E_m, J_m) \cdot k_{1,\infty}(T) \cdot [HO_2] \cdot [CH_3O_2], \quad (11)$$

where $k_{3,\infty}(T)$ is the *capture rate constant*—that can be calculated using micro-variational transition state theory ($\mu\nu$ TST) [47–50] (see Equation (13) below)—for the barrier-less association step of HO₂ and CH₃O₂ leading to triplet PRC. $F_3(E_m, J_m)$ is the E, J -resolved initial distribution function for the nascent energized triplet PRC and given by [43,46]:

$$F_3(E_m, J_m) = \frac{(2J_m+1) \cdot k_{3 \rightarrow \text{CH}_3\text{O}_2}(E_m, J_m) \cdot \rho_3(E_m, J_m) \cdot \exp(-E_m/RT)}{\sum_{J_m=0}^{J_m^{\max}} (2J_m+1) \int_{E_i=0}^{E_i^{\max}} k_{3 \rightarrow \text{CH}_3\text{O}_2}(E_m, J_m) \cdot \rho_3(E_m, J_m) \cdot \exp(-E_m/RT) \cdot dE_m} \quad (12)$$

In Equation (12), $\rho_3(E_m, J_m)$ is the density of ro-vibrational states for triplet PRC, and $k_{3 \rightarrow \text{CH}_3\text{O}_2}(E_m, J_m)$ is the microcanonical rate constant for the triplet PRC \rightarrow HO₂ + CH₃O₂ step, which is calculated using micro-variational TST [50,51].

$$k_{3,\infty}(T) = \frac{\sigma}{h} \times \frac{Q_{tr}^{\neq} Q_e^{\neq}}{Q_{\text{HO}_2}^{\text{re}} \cdot Q_{\text{CH}_3\text{O}_2}^{\text{re}}} \times \sum_{J=0}^{\infty} (2J+1) \int_0^{\infty} \text{Min}[G_{rv}^{\neq}(E, J)] \times \exp(-E/k_B T) dE \quad (13)$$

Here, h is Planck's constant, k_B is Boltzmann's constant, and σ is the reaction path degeneracy, which is equal to $3 \times 2/2 \pm 2 = 3/2$ for the triplet PES in this case, 2 on the nominator is because TS1 is a chiral structure. Note that electronic partition functions for all stationary points are set to 1, 2, and 3 for singlet, doublet and triplet electronic states, respectively. T is the reaction temperature and E is the total internal energy. $\text{Min}[G_{rv}^{\neq}(E, J)]$ stands for minimizing the chemical reaction flux at the given E and J . $Q_{\text{HO}_2}^{\text{re}}$ and $Q_{\text{CH}_3\text{O}_2}^{\text{re}}$ are the complete partition functions for HO₂ and CH₃O₂, respectively. Q_{tr} is the translational partition function, and Q_e is the electronic partition function of the TS (the superscripts "re" and " \neq " designate reactants and transition state (TS), respectively). G_{rv}^{\neq} is the sum of ro-vibrational quantum states of the TS for the given E and J , which can be obtained from its vibrational counterpart using the J -shifting approximation [52–54], Equations (14) and (15):

$$G_{rv}^{\neq}(E, J) = \sum_{K=-J}^{K=+J} G_v^{\neq}(E - E_r(J, K)) \quad (14)$$

$$\rho_{rv}(E, J) = \sum_{K=-J}^{K=+J} \rho_v(E - E_r(J, K)) \quad (15)$$

In Equation (14), G_v^{\neq} is the anharmonic (coupled) vibrational sum of states of TS that is calculated using Miller's semiclassical TST (SCTST) theory [55–59] based on the Wang–Landau algorithm [60–63]. SCTST theory [55–59] automatically includes coupled anharmonic vibrations and multidimensional quantum mechanical tunneling. E_r is the (external) rotational energy level of TS, which is approximated by a symmetric top, [64] Equation (16):

$$E_r(J, K) = J(J+1)\bar{B} + (A - \bar{B})K^2, \text{ with } \bar{B} = \sqrt{B \cdot C} \text{ and } -J \leq K \leq +J \quad (16)$$

In this work, hindered internal rotations with low vibrational frequencies in stationary points are separated and approximately treated as separable one-dimensional hindered internal rotors (1DHR). We then solve 1D Schrodinger equation independently to obtain a spectrum of eigenvalues for each 1DHR mode, whose sums of quantum states are then counted directly. Finally, we convolve these 1DHR motions with the remaining vibrations to obtain the overall density of vibrational states.

The phenomenological rate coefficients can be determined in two ways. First, they can be associated with the lowest (negative) eigenvalues (i.e., chemically significant eigenvalues, CSE) that are obtained by solving Equations (8) and (9). Second, the rate coefficients can also be calculated at a pseudo steady-state condition using Equations (17) and (18):

$$k_3(T, p) = \left(1 - \gamma_3^{\text{HO}_2}\right) \times k_{3,\infty}(T), \text{ for the triplet PES} \quad (17)$$

$$k_1(T, p) = (1 - \gamma_1^{HO_2}) \times k_{1,\infty}(T), \text{ for the singlet PES} \quad (18)$$

$$k_{overall}(T, p) = k_3(T, p) + k_1(T, p) \quad (19)$$

In Equations (17) and (18), γ^{HO_2} is the mole fraction of HO₂, which is produced by unimolecular re-dissociation of the triplet (or singlet) energized PRC back to initial reactants (HO₂ and CH₃O₂), obtained at a pseudo steady state condition at a given T and p .

3. Results and Discussions

3.1. Reaction Mechanisms

The association of HO₂ and CH₃O₂ can proceed on both the triplet and singlet electronic state PESs. The reaction pathways on the triplet PES are displayed on the right-hand side of Figure 1 while those on the singlet PES are presented on the left-hand side.

On the triplet PES: the barrier-less association of HO₂ and CH₃O₂ leads to the formation of the vibrationally excited triplet pre-reactive complex (³PRC), which is a van der Waals complex stabilized by two H-bonds with a binding energy of 5.92 kcal mol⁻¹. Starting at ³PRC, there are two feasible dissociating pathways: it can re-dissociate back to the initial reactants (HO₂ + CH₃O₂) or it can carry out the internal H-abstraction from HO₂ to yield CH₃OOH and triplet O₂. The latter pathway has a submerged barrier of -2.77 kcal mol⁻¹ (relative to reactants), and thus formation of products is facile. This is the major (if not sole) product pathway, which was previously confirmed by both experimental [9–19] and theoretical [20,22] studies. It should be noted that HO₂ could abstract an H atom from the CH₃ group of CH₃O₂ leading to H₂O₂ and triplet CH₂OO, but this H-abstraction pathway (not shown in Figure 1) has a very high barrier of ca. 28.6 kcal mol⁻¹ at mHEAT method, and can be safely disregarded.

On the singlet PES: the barrier-less combination of HO₂ and CH₃O₂ can also lead to an energized singlet adduct, ¹PRC. Because the two unpaired electrons in PRC are far apart, their interaction is extremely weak. As a result, the binding energy of ¹PRC (5.92 kcal mol⁻¹) is nearly identical to that of ³PRC. When formed, ¹PRC can carry out three plausible dissociative pathways. First, it can return without a potential barrier to the initial reactants. Second, it can undergo an O–O association via TS3 to lead to vibrationally excited methyl tetraoxide (MTO), overcoming a barrier of 5.77 kcal mol⁻¹. When produced, MTO mostly isomerizes back to ¹PRC because further decomposition of MTO yielding various products must overcome much higher barriers (not shown in Figure 1), which are therefore irrelevant under the conditions studied here. Third, it can do an internal H abstraction via TS2 to make CH₃OOH and singlet O₂, surmounting a barrier of 5.79 kcal mol⁻¹. It is worthy of mention that, in addition to the triplet channel, this singlet channel provides an additional contribution (about 10%) to the overall formation of CH₃OOH observed in experiments. To the best of our knowledge, this new finding has not previously been reported in the literature.

3.2. Statistical Kinetics Analysis

To solve a master equation, one must have the collisional parameters of energized adduct (CH₄O₄) and bath gas (both N₂ and He used here) as well as the energy/angular momentum transfer probability distribution function. These parameters were empirically selected based on similar (known) systems [65] and are tabulated in Table S2. It is worth mentioning that the calculated rate constants in this work depend only slightly on pressure (see Figure 2), at pressures typical of atmospheric conditions ($p \leq 760$ Torr), they are practically constant, as seen in Figure 2.

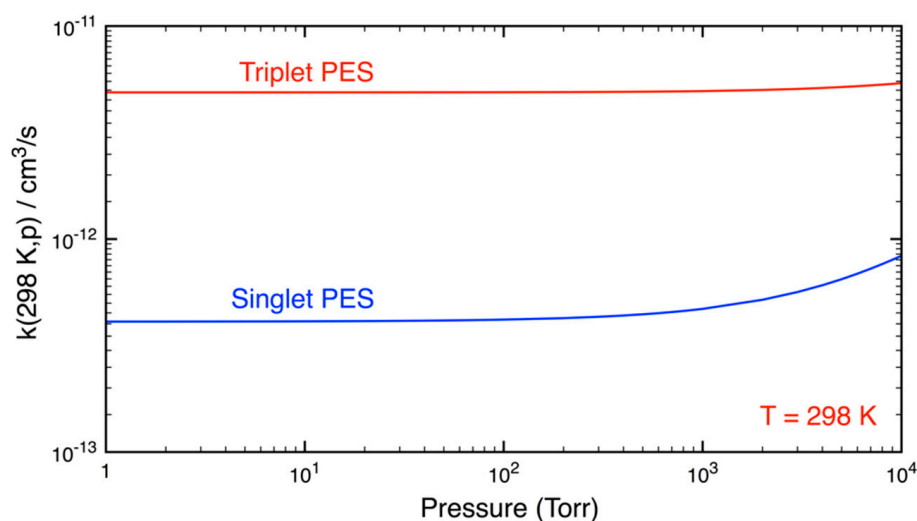


Figure 2. Two falloff curves for the reaction of HO_2 and CH_3O_2 calculated at $T = 298$ K and a function of pressure.

Figure 2 shows two falloff curves calculated at $T = 298$ K. The reaction on the triplet PES appeared to be pressure-independent (for $p = 1$ – $10,000$ Torr) while that on the singlet PES depended slightly on pressure when P was greater than 1000 Torr. These results are completely consistent with experimental results, which show that the reaction does not depend on pressure when $p \leq 760$ Torr.

To examine the formation of methyl tetraoxide (MTO), mole fractions of various species from the reaction on the singlet PES were computed at 298 K and a function of pressure. As revealed in Figure 3, the yield of the thermalized MTO—which is formed through collisional stabilization—was negligible ($<0.1\%$) even at $p = 10,000$ Torr. There are two reasons for this observation: first, the chemical flux via the tighter TS3 is about two orders of magnitude smaller than that proceeding via the looser TS2; second, the energized intermediate MTO, when produced, prefers to isomerize back to ^1PRC .

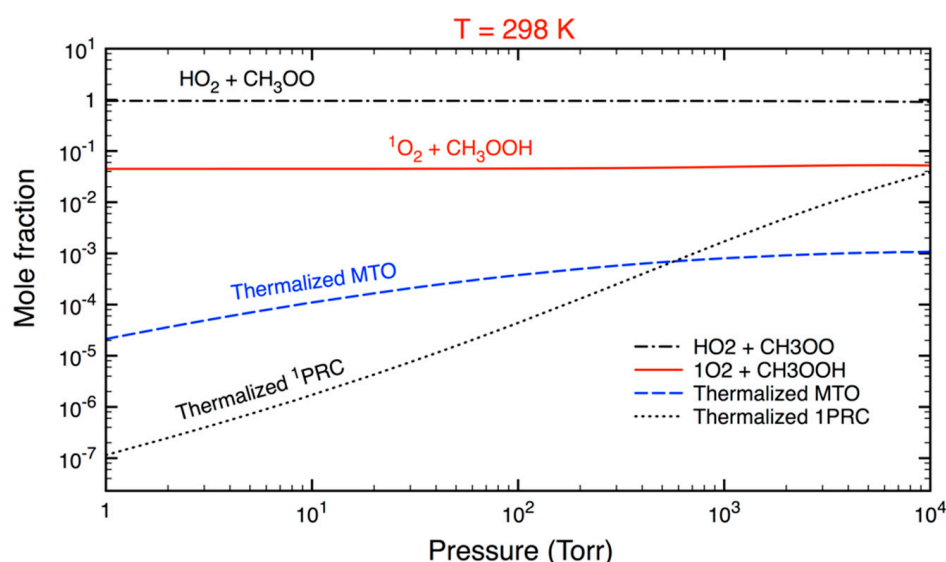


Figure 3. Mole fractions of various species in the reaction of HO_2 and CH_3O_2 occurring on the singlet electronic state PES, calculated at $T = 298$ K and a function of pressure.

Figure 3 also indicates that most of vibrationally excited ^1PRC , when formed, returned to initial reactants ($\text{HO}_2 + \text{CH}_3\text{O}_2$) while the rest further reacted to yield CH_3OOH and singlet O_2 . Furthermore, the yield of collisional stabilization of ^1PRC was found to be

minor, especially at atmospheric pressures. It can be predicted that the thermalized ^1PRC decreases significantly at higher temperatures in combustion environments. In practical applications, the reaction pathway on the singlet PES must be considered at the low-P limit as well. This finding differs from a previous theoretical study [22] where the high-P limit model (i.e., the thermal equilibrium was assumed) was used to compute $k(T)$, which would appear to be inappropriate.

The results from the master equation analysis show that CH_3OOH is the sole product under the conditions considered in this work. Importantly, CH_3OOH can be produced from both the triplet and singlet PESs with a relative ratio of about 9:1, which is found to be very marginally dependent on temperature (see Figure 4). The yield of CH_3OOH from the triplet PES is dominant for two reasons: first, the formation rate of ^3PRC is three times as fast as that of ^1PRC , due to the electronic degeneracy; and second, TS1 lies lower in energy than TS2.

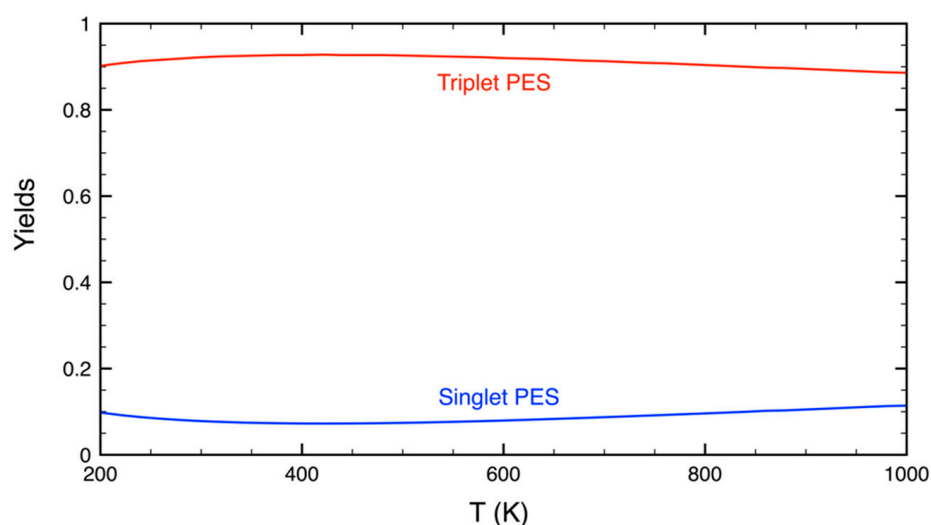


Figure 4. A comparison of the yield of CH_3OOH produced from the triplet and singlet PESs as a function of temperature.

Figure 5 shows the reaction rate coefficients calculated as a function of temperature, experimental data in symbols are also included for comparison. An inspection of Figure 5 reveals that the ab initio $k(T)$ results (the dashed blue curve) were in good agreement with experiments at low temperatures ($T < 260$ K), but slightly too low at higher temperatures. By lowering the calculated barriers by $0.5 \text{ kcal mol}^{-1}$, which is within the range of error expected with the mHEAT method, we were able to reproduce most experimental data within 20% (see the red solid curve). Combining the high-level theoretical results obtained in this work and available experimental data, we carried out curve fitting and obtained an Arrhenius equation:

$$k(T) = 2.75 \times 10^{-13} \times e^{+1.75 \text{ kcal mol}^{-1}/RT}, \text{ in cm}^3/\text{s}, \text{ for } T = 200\text{--}800 \text{ K} \quad (20)$$

As seen in Figure 6, Equation (20) presents a new set of predicted reaction rate constants, which agree well (within 10%) with most experimental data where they are available. In addition, it provides reliable rate constants where experimental data are absent. Therefore, we believe that Equation (20) can be useful for kinetics modeling.

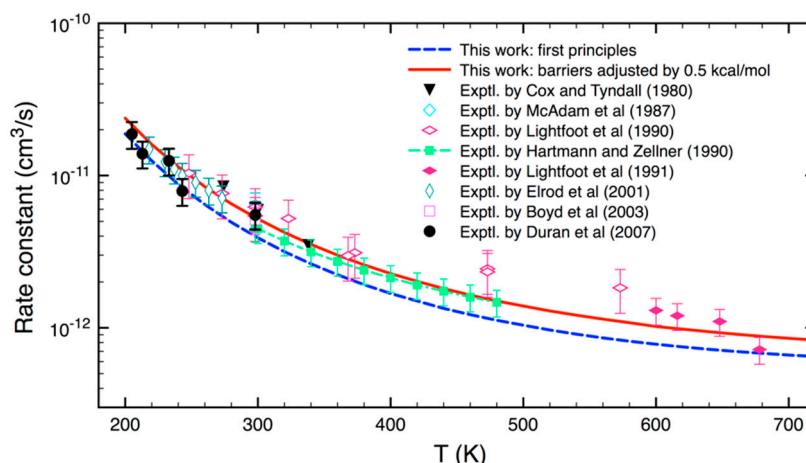


Figure 5. Calculated thermal rate coefficients for the reaction of HO_2 and CH_3O_2 : ab initio $k(T)$: dashed blue curve; the barriers lessened by $0.5 \text{ kcal mol}^{-1}$: solid red curve. Experimental data (symbols) are also included for comparison.

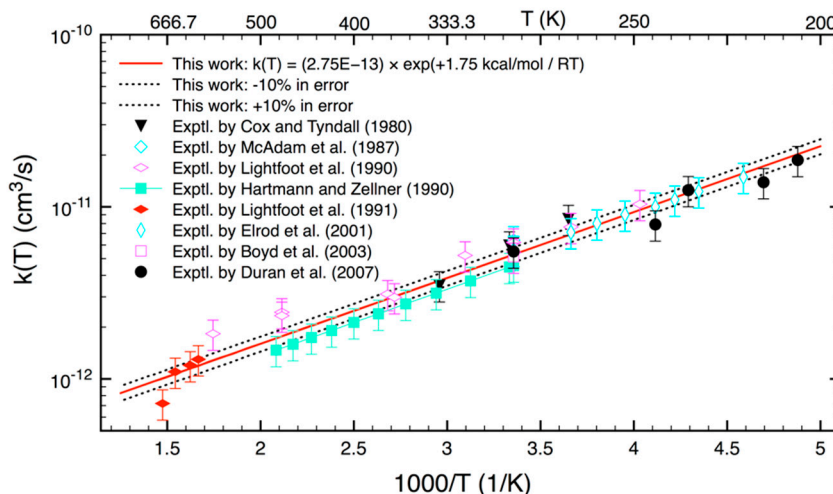


Figure 6. The reaction rate coefficients (the solid red curve) for the reaction of HO_2 and CH_3O_2 are recommended in this work. Experimental data (symbols) are also included for comparison.

4. Conclusions

The reaction of HO_2 and CH_3O_2 was reinvestigated using high-accuracy coupled-cluster calculations, followed by computing phenomenological rate coefficients with an E,J-resolved master equation technique. Methyl hydroperoxide (CH_3OOH) was found to be the sole product and can be produced from both triplet and singlet PESs with a ratio of about 9:1, a factor which is nearly independent on temperature and pressure. The formation of CH_3OOH on the singlet PES is a new finding in this work. The yield of methyl tetraoxide (CH_3OOOOH) from the singlet PES formed through collisional stabilization was found to be negligibly small. Formaldehyde (CH_2O) was not found to be a primary product; if formed, it is most likely via succeeding photo-oxidation processes of CH_3OOH in some experiments. The reaction was found to proceed through hydrogen-bonded pre-reactive complexes, followed by internal H-abstraction steps via submerged barriers leading to products, thus the reaction rate constant had a slight negative temperature dependence and did not depend on pressure (when $p \leq 1 \text{ atm}$). The rate coefficients fitted to the expression of $k(T) = 2.75 \times 10^{-13} \times e^{+1.75 \text{ kcal mol}^{-1}/RT}$ (in cm^3/s) for a temperature range of 200–800 K are recommended for kinetics modeling. These findings are completely consistent with experimental knowledge on this system.

Supplementary Materials: The following supporting information can be downloaded at: <https://www.mdpi.com/article/10.3390/atmos13091397/s1>.

Author Contributions: The original manuscript was prepared by T.L.N. It was reviewed and edited by J.F.S. All authors have read and agreed to the published version of the manuscript.

Funding: This work was supported by the U.S. Department of Energy, Office of Basic Energy Sciences under Award DE-SC0018164.

Acknowledgments: We would like to thank two anonymous reviewers who provided helpful comments that helped to improve the presentation of this work.

Conflicts of Interest: The authors declare no conflict of interest.

References

1. Atkinson, R. Gas-Phase Tropospheric Chemistry of Volatile Organic Compounds: 1. Alkanes and Alkenes. *J. Phys. Chem. Ref. Data* **1997**, *26*, 215–290. [[CrossRef](#)]
2. Miller, J.A.; Pilling, M.J.; Troe, E. Unravelling combustion mechanisms through a quantitative understanding of elementary reactions. *Proc. Combust. Inst.* **2005**, *30*, 43–88.
3. Baulch, D.L.; Bowman, C.T.; Cobos, C.J.; Cox, R.A.; Just, T.; Kerr, J.A.; Pilling, M.J.; Stocker, D.; Troe, J.; Tsang, W.; et al. Evaluated kinetic data for combustion modeling: Supplement II. *J. Phys. Chem. Ref. Data* **2005**, *34*, 757–1397.
4. Orlando, J.J.; Tyndall, G.S. Laboratory studies of organic peroxy radical chemistry: An overview with emphasis on recent issues of atmospheric significance. *Chem. Soc. Rev.* **2012**, *41*, 6294–6317.
5. Wallington, T.J.; Dagaut, P.; Kurylo, M.J. Ultraviolet-Absorption Cross-Sections and Reaction-Kinetics and Mechanisms for Peroxy-Radicals in the Gas-Phase. *Chem. Rev.* **1992**, *92*, 667–710.
6. Tyndall, G.S.; Cox, R.A.; Granier, C.; Lesclaux, R.; Moortgat, G.K.; Pilling, M.J.; Ravishankara, A.R.; Wallington, T.J. Atmospheric chemistry of small organic peroxy radicals. *J. Geophys. Res.-Atmos* **2001**, *106*, 12157–12182.
7. Lightfoot, P.D.; Cox, R.A.; Crowley, J.N.; Destriau, M.; Hayman, G.D.; Jenkin, M.E.; Moortgat, G.K.; Zabel, F. Organic Peroxy-Radicals-Kinetics, Spectroscopy and Tropospheric Chemistry. *Atmos. Environ. Part A Gen. Top.* **1992**, *26*, 1805–1961.
8. Onel, L.; Brennan, A.; Seakins, P.W.; Whalley, L.; Heard, D.E. A new method for atmospheric detection of the CH_3O_2 radical. *Atmos. Meas. Tech.* **2017**, *10*, 3985–4000.
9. Cox, R.A.; Tyndall, G.S. Rate Constants for the Reactions of CH_3O_2 with HO_2 , NO and NO_2 Using Molecular Modulation Spectrometry. *J. Chem. Soc. Faraday Trans.* **1980**, *76*, 153–163.
10. Kurylo, M.J.; Dagaut, P.; Wallington, T.J.; Neuman, D.M. Kinetic Measurements of the Gas-Phase $\text{HO}_2 + \text{CH}_3\text{O}_2$ Cross-Disproportionation Reaction at 298-K. *Chem. Phys. Lett.* **1987**, *139*, 513–518.
11. Mcadam, K.; Veyret, B.; Lesclaux, R. UV Absorption-Spectra of HO_2 and CH_3O_2 Radicals and the Kinetics of Their Mutual Reactions at 298-K. *Chem. Phys. Lett.* **1987**, *133*, 39–44.
12. Jenkin, M.E.; Cox, R.A.; Hayman, G.D.; Whyte, L.J. Kinetic-Study of the Reactions $\text{CH}_3\text{O}_2 + \text{CH}_3\text{O}_2$ and $\text{CH}_3\text{O}_2 + \text{HO}_2$ Using Molecular Modulation Spectroscopy. *J. Chem. Soc. Faraday Trans.* **1988**, *84*, 913–930.
13. Wallington, T.J. Fourier-Transform Infrared Product Study of the Reaction of $\text{CH}_3\text{O}_2 + \text{HO}_2$ over the Pressure Range 15–700 Torr at 295-K. *J. Chem. Soc. Faraday Trans.* **1991**, *87*, 2379–2382.
14. Lightfoot, P.D.; Roussel, P.; Caralp, F.; Lesclaux, R. Flash-Photolysis Study of the $\text{CH}_3\text{O}_2 + \text{CH}_3\text{O}_2$ and $\text{CH}_3\text{O}_2 + \text{HO}_2$ Reactions between 60-K and 719-K-Unimolecular Decomposition of Methylhydroperoxide. *J. Chem. Soc. Faraday Trans.* **1991**, *87*, 3213–3220.
15. Lightfoot, P.D.; Veyret, B.; Lesclaux, R. Flash-Photolysis Study of the $\text{CH}_3\text{O}_2 + \text{HO}_2$ Reaction between 248 and 573-K. *J. Phys. Chem.* **1990**, *94*, 708–714. [[CrossRef](#)]
16. Boyd, A.A.; Flaud, P.M.; Daugey, N.; Lesclaux, R. Rate constants for $\text{RO}_2 + \text{HO}_2$ reactions measured under a large excess of HO_2 . *J. Phys. Chem. A* **2003**, *107*, 818–821.
17. Raventos-Duran, M.T.; McGillen, M.; Percival, C.J.; Hamer, P.D.; Shallcross, D.E. Kinetics of the $\text{CH}_3\text{O}_2 + \text{HO}_2$ reaction: A temperature and pressure dependence study using chemical ionization mass Spectrometry. *Int. J. Chem. Kinet.* **2007**, *39*, 571–579.
18. Moortgat, G.K.; Cox, R.A.; Schuster, G.; Burrows, J.P.; Tyndall, G.S. Peroxy Radical Reactions in the Photo-Oxidation of CH_3CHO . *J. Chem. Soc. Faraday Trans.* **1989**, *85*, 809–829.
19. Elrod, M.J.; Ranschaert, D.L.; Schneider, N.J. Direct kinetics study of the temperature dependence of the CH_2O branching channel for the $\text{CH}_3\text{O}_2 + \text{HO}_2$ reaction. *Int. J. Chem. Kinet.* **2001**, *33*, 363–376.
20. Hou, H.; Wang, B.S. A systematic computational study on the reactions of HO_2 with RO_2 : The $\text{HO}_2 + \text{CH}_3\text{O}_2$ (CD_3O_2) and $\text{HO}_2 + \text{CH}_2\text{FO}_2$ reactions. *J. Phys. Chem. A* **2005**, *109*, 451–460.
21. Drougas, E. Quantum mechanical studies of the $\text{CH}_3\text{O}_2 + \text{HO}_2$ reaction. *Comput. Theor. Chem.* **2016**, *1093*, 98–103.
22. Anglada, J.M.; Olivella, S.; Sole, A. Mechanistic study of the $\text{CH}_3\text{O}_2 + \text{HO}_2 \rightarrow \text{CH}_3\text{O}_2\text{H} + \text{O}_2$ reaction in the gas phase. Computational evidence for the formation of a hydrogen-bonded diradical complex. *J. Phys. Chem. A* **2006**, *110*, 6073–6082. [[PubMed](#)]
23. Zhang, T.L.; Wang, W.L.; Zhang, P.; Lu, J.; Zhang, Y. Water-catalyzed gas-phase hydrogen abstraction reactions of CH_3O_2 and HO_2 with HO_2 : A computational investigation. *Phys. Chem. Chem. Phys.* **2011**, *13*, 20794–20805. [[PubMed](#)]

24. English, A.M.; Hansen, J.C.; Szente, J.J.; Maricq, A.M. The effects of water vapor on the CH_3O_2 self-reaction and reaction with HO_2 . *J. Phys. Chem. A* **2008**, *112*, 9220–9228. [[PubMed](#)]
25. Raghavachari, K.; Trucks, G.W.; Pople, J.A.; Headgordon, M. A 5th-Order Perturbation Comparison of Electron Correlation Theories. *Chem. Phys. Lett.* **1989**, *157*, 479–483.
26. Bartlett, R.J.; Watts, J.D.; Kucharski, S.A.; Noga, J. Noniterative 5th-Order Triple and Quadruple Excitation-Energy Corrections in Correlated Methods. *Chem. Phys. Lett.* **1990**, *165*, 513–522.
27. Stanton, J.F. Why CCSD(T) works: A different perspective. *Chem. Phys. Lett.* **1997**, *281*, 130–134.
28. Almlöf, J.; Taylor, P.R. General Contraction of Gaussian-Basis Sets. 1. Atomic Natural Orbitals for 1st-Row and 2nd-Row Atoms. *J. Chem. Phys.* **1987**, *86*, 4070–4077.
29. Almlöf, J.; Taylor, P.R. General Contraction of Gaussian-Basis Sets. 2. Atomic Natural Orbitals and the Calculation of Atomic and Molecular-Properties. *J. Chem. Phys.* **1990**, *92*, 551–560. [[CrossRef](#)]
30. Dunning, T.H. Gaussian-Basis Sets for Use in Correlated Molecular Calculations. 1. The Atoms Boron through Neon and Hydrogen. *J. Chem. Phys.* **1989**, *90*, 1007–1023.
31. Thorpe, J.H.; Lopez, C.A.; Nguyen, T.L.; Baraban, J.H.; Bross, D.H.; Ruscic, B.; Stanton, J.F. High-accuracy extrapolated ab initio thermochemistry. IV. A modified recipe for computational efficiency. *J. Chem. Phys.* **2019**, *150*, 224102. [[CrossRef](#)] [[PubMed](#)]
32. Ruscic, B.; Bross, D.H. Active Thermochemical Tables (ATcT) Values Based on Ver. 1.122r of the Thermochemical Network 2022. Available online: ATcT.anl.gov (accessed on 4 July 2022).
33. Jeffery, S.J.; Gates, K.E.; Smith, S.C. Full Iterative Solution of the Two-Dimensional Master Equation for Thermal Unimolecular Reactions. *J. Phys. Chem.* **1996**, *100*, 7090–7096. [[CrossRef](#)]
34. Robertson, S.H.; Pilling, M.J.; Green, N.J.B. Diffusion approximations of the two-dimensional master equation. *Mol. Phys.* **1996**, *89*, 1531–1551. [[CrossRef](#)]
35. Miller, J.A.; Klippenstein, S.J.; Raffy, C. Solution of Some One- and Two-Dimensional Master Equation Models for Thermal Dissociation: The Dissociation of Methane in the Low-Pressure Limit. *J. Phys. Chem.* **2002**, *106*, 4904–4913. [[CrossRef](#)]
36. Jasper, A.W.; Pelzer, K.M.; Miller, J.A.; Kamarchik, E.; Harding, L.B.; Klippenstein, S.J. Predictive a priori pressure-dependent kinetics. *Science* **2014**, *346*, 1212–1215. [[CrossRef](#)] [[PubMed](#)]
37. Nguyen, T.L.; Stanton, J.F. A Steady-State Approximation to the Two-Dimensional Master Equation for Chemical Kinetics Calculations. *J. Phys. Chem. A* **2015**, *119*, 7627–7636. [[CrossRef](#)]
38. Nguyen, T.L.; Lee, H.; Matthews, D.A.; McCarthy, M.C.; Stanton, J.F. Stabilization of the Simplest Criegee Intermediate from the Reaction between Ozone and Ethylene: A High-Level Quantum Chemical and Kinetic Analysis of Ozonolysis. *J. Phys. Chem. A* **2015**, *119*, 5524–5533.
39. Nguyen, T.L.; Stanton, J.F. Pragmatic Solution for a Fully E,J-Resolved Master Equation. *J. Phys. Chem. A* **2020**, *124*, 2907–2918. [[CrossRef](#)]
40. Troe, J. Theory of Thermal Unimolecular Reactions at Low-Pressures.1. Solutions of Master Equation. *J. Chem. Phys.* **1977**, *66*, 4745–4757. [[CrossRef](#)]
41. Reid, R.C.; Prausnitz, J.M.; Sherwood, T.K. *The Properties of Gases and Liquids*; McGraw-Hill: New York, NY, USA, 1977.
42. Neufeld, P.D.; Aziz, R.A.; Janzen, A.R. Empirical Equations to Calculate 16 of Transport Collision Integrals-Omega(L, S) for Lennard-Jones (12-6) Potential. *J. Chem. Phys.* **1972**, *57*, 1100. [[CrossRef](#)]
43. Holbrook, K.A.; Pilling, M.J.; Robertson, S.H.; Robinson, P.J. *Unimolecular Reactions*, 2nd ed.; Wiley: Chichester, UK; New York, NY, USA, 1996; 417p.
44. Gilbert, R.G.; Smith, S.C. *Theory of Unimolecular and Recombination Reactions*; Blackwell Science Publications; Publishers' Business Services Distributor: Oxford, UK; Boston, MA, USA, 1990; 356p.
45. Forst, W. Adiabatic Rotations in Unimolecular Rate Theory. *J. Chem. Phys.* **1968**, *48*, 3665. [[CrossRef](#)]
46. Forst, W. *Unimolecular Reactions: A Concise Introduction*; Cambridge University Press: Cambridge, UK; New York, NY, USA, 2003; 319p.
47. Eyring, H. The activated complex in chemical reactions. *J. Chem. Phys.* **1935**, *3*, 107–115. [[CrossRef](#)]
48. Evans, M.G.; Polanyi, M. Some applications of the transition state method to the calculation of reaction velocities, especially in solution. *Trans. Faraday Soc.* **1935**, *31*, 0875–0893. [[CrossRef](#)]
49. Truhlar, D.G.; Garrett, B.C.; Klippenstein, S.J. Current status of transition-state theory. *J. Phys. Chem.* **1996**, *100*, 12771–12800. [[CrossRef](#)]
50. Hase, W.L. Variational Unimolecular Rate Theory. *Acc. Chem. Res.* **1983**, *16*, 258–264. [[CrossRef](#)]
51. Truhlar, D.G.; Garrett, B.C. Variational Transition-State Theory. *Annu. Rev. Phys. Chem.* **1984**, *35*, 159–189. [[CrossRef](#)]
52. Miller, W.H. Tunneling Corrections to Unimolecular Rate Constants, with Application to Formaldehyde. *J. Am. Chem. Soc.* **1979**, *101*, 6810–6814. [[CrossRef](#)]
53. Bowman, J.M. Reduced Dimensionality Theory of Quantum Reactive Scattering. *J. Phys. Chem.* **1991**, *95*, 4960–4968. [[CrossRef](#)]
54. Balakrishnan, N. Quantum mechanical investigation of the $\text{O} + \text{H}_2 \rightarrow \text{OH} + \text{H}$ reaction. *J. Chem. Phys.* **2003**, *119*, 195–199. [[CrossRef](#)]
55. Miller, W.H. Semiclassical Theory for Non-Separable Systems—Construction of Good Action-Angle Variables for Reaction-Rate Constants. *Faraday Discuss.* **1977**, *62*, 40–46. [[CrossRef](#)]

56. Miller, W.H.; Hernandez, R.; Handy, N.C.; Jayatilaka, D.; Willetts, A. Abinitio Calculation of Anharmonic Constants for a Transition-State, with Application to Semiclassical Transition-State Tunneling Probabilities. *Chem. Phys. Lett.* **1990**, *172*, 62–68. [[CrossRef](#)]
57. Hernandez, R.; Miller, W.H. Semiclassical Transition-State Theory—a New Perspective. *Chem. Phys. Lett.* **1993**, *214*, 129–136. [[CrossRef](#)]
58. Nguyen, T.L.; Stanton, J.F.; Barker, J.R. A practical implementation of semi-classical transition state theory for polyatomics. *Chem. Phys. Lett.* **2010**, *499*, 9–15. [[CrossRef](#)]
59. Nguyen, T.L.; Stanton, J.F.; Barker, J.R. Ab Initio Reaction Rate Constants Computed Using Semiclassical Transition-State Theory: HO + H₂ → H₂O + H and Isotopologues. *J. Phys. Chem. A* **2011**, *115*, 5118–5126. [[CrossRef](#)]
60. Wang, F.G.; Landau, D.P. Efficient, multiple-range random walk algorithm to calculate the density of states. *Phys. Rev. Lett.* **2001**, *86*, 2050–2053. [[CrossRef](#)]
61. Wang, F.G.; Landau, D.P. Determining the density of states for classical statistical models: A random walk algorithm to produce a flat histogram. *Phys. Rev. E* **2001**, *64*, 056101. [[CrossRef](#)]
62. Basire, M.; Parneix, P.; Calvo, F. Quantum anharmonic densities of states using the Wang-Landau method. *J. Chem. Phys.* **2008**, *129*, 081101. [[CrossRef](#)]
63. Nguyen, T.L.; Barker, J.R. Sums and Densities of Fully Coupled Anharmonic Vibrational States: A Comparison of Three Practical Methods. *J. Phys. Chem. A* **2010**, *114*, 3718–3730. [[CrossRef](#)]
64. Baer, T.; Hase, W.L. *Unimolecular Reaction Dynamics: Theory and Experiments*; Oxford University Press: New York, NY, USA, 1996; 438p.
65. Barker, J.R.; Nguyen, T.L.; Stanton, J.F.; Aieta, C.; Ceotto, M.; Gabas, F.; Kumar, T.J.D.; Li, C.G.L.; Lohr, L.L.; Maranzana, A.; et al. MULTIWELL Program Suite, Climate and Space Sciences and Engineering, University of Michigan. *Ann. Arbor, MI* **2021**.